
Learning Distributed Geometric Koopman Operator for Sparse Networked Dynamical Systems

Anonymous Author(s)

Anonymous Affiliation

Anonymous Email

Abstract

1
2 The Koopman operator theory provides an alternative to studying nonlinear net-
3 worked dynamical systems (NDS) by mapping the state space to an abstract higher
4 dimensional space where the system evolution is linear. The recent works show
5 the application of graph neural networks (GNNs) to learn state to object-centric
6 embedding and achieve centralized block-wise computation of the Koopman oper-
7 ator (KO) under additional assumptions on the underlying node properties and
8 constraints on the KO structure. However, the computational complexity of learn-
9 ing the Koopman operator increases for large NDS. Moreover, the computational
10 complexity increases in a combinatorial fashion with the increase in number of
11 nodes. The learning challenge is further amplified for sparse networks by two
12 factors: 1) sample sparsity for learning the Koopman operator in the non-linear
13 space, and 2) the dissimilarity in the dynamics of individual nodes or from one
14 subgraph to another. Our work aims to address these challenges by formulating
15 the representation learning of NDS into a multi-agent paradigm and learning the
16 Koopman operator in a distributive manner. Our theoretical results show that the
17 proposed distributed computation of the geometric Koopman operator is beneficial
18 for sparse NDS, whereas for the fully connected systems this approach coincides
19 with the centralized one. The empirical study on a rope system, a network of
20 oscillators, and a power grid show comparable and superior performance along
21 with computational benefits with the state-of-the-art methods.

22 1 Introduction

23 NDS represents an important class of dynamic networks where the state of the network is defined by
24 a vector of node-level properties in a geometrical manifold, and their evolution is governed by a set
25 of differential equations. Data-driven modeling of both spatio-temporal dependencies and evolution
26 dynamics is essential to predict the response of the NDS to an external perturbation. Surely, machine-
27 learning approaches that explicitly recognize the interconnection structure of such systems or model
28 the dynamical system-driven evolution of the network outperform initial deep learning approaches
29 based on recurrent neural networks and its variants [1–5]. Deep learning approaches such as GNNs
30 fit into this paradigm by learning non-linear functions for each of the encoder-system model-decoder
31 components [6–10]. Discovering the underlying physics of dynamical systems have intrigued control
32 theory researcher for decades resulting into multiple sub-space based system identification works
33 [11–14]. Koopman operator theory [15, 16] is an approach for such model discovery where the core
34 idea is to transform the observed state-space variables to the space of square-integrable functions,
35 where a linear operator provides an exact representation of the underlying dynamical system and the
36 spectrum of the operator encodes all the non-linear behaviors. However, for computational purposes,
37 finding finite-dimensional approximation of Koopman operator is challenging. The key to computing
38 the finite-dimensional Koopman operator is fixing the lifting functions (observables) and existing
39 approaches such as classical or extended dynamic mode decomposition [17, 18] use an a-priori
40 choice of basis functions for lifting; however, this choice usually fails to generalize to more complex
41 environments. Instead, learning these transformations from the system trajectories themselves using
42 deep neural networks (DNNs) have been shown to yield much richer invariant subspaces [19, 20].

43 Continuing the idea of lifting the non-linear state space into another space to learn linear transition
 44 dynamics, [21] proposed the use of a graph neural network as the encoder-decoder function. While
 45 graph neural networks (GNN) [22] appears to be a natural approach for modeling the physics of
 46 networked systems, their ability to discover dynamic evolution models of large-scale networked
 47 systems is a nascent area of research [6, 7, 9, 23]. For NDS, where the number of system states
 48 increases with the number of nodes, the computational complexity of learning the Koopman operator
 49 also increases. The topology of the network or its sparsity are typically not taken advantage of in the
 50 existing studies when learning observable functions or the Koopman operator.

51 In this work, we address the challenge of learning dissimilar dynamics in sparse networks by
 52 formulating the representation learning of networked dynamical systems into a multi-agent paradigm.
 53 We refer to this approach as Distributed Koopman-GNN (DKGNN). DKGNN is more suitable for
 54 sparse and large networked dynamical systems as the proposed distributed learning method yields
 55 superior computational efficiency compared to traditional methods. We apply the GNNs to capture
 56 the distributed nature of the dynamical system behavior, transform the original state-space into
 57 the Koopman observable space, and subsequently use the network sparsity patterns to constrain
 58 the Koopman operator construction into a block-structured distributed representation along with
 59 theoretical guarantees. Information-theoretic network clustering strategies were utilized for specific
 60 dynamic systems to capture the joint evolution of the clusters in a coarse-grained fashion resulting in
 further computational benefits. Please see Figure 1 for an illustration of the approach.

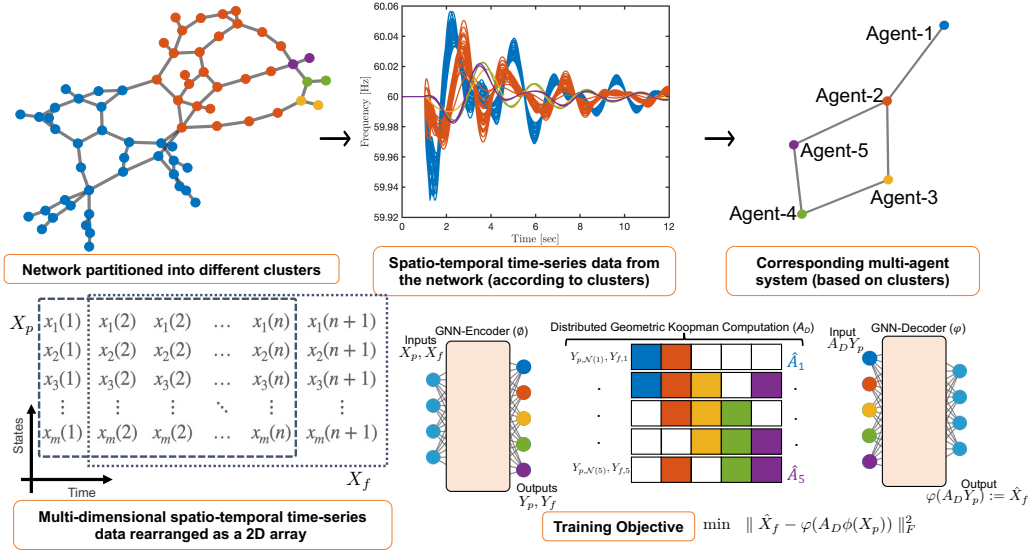


Figure 1: Overview of the proposed approach (best viewed with colors) : (Top row) the sparse networked dynamical system (NDS) is partitioned into clusters using dynamic spatio-temporal data resulting into an agent representation (each color represents an agent). The time-series associated with each node is also color coded by the agents. (Bottom row) the re-arranged multi-dimensional spatio-temporal data is fed to the GNN along with the agent network structure to learn the nonlinear observables. Learning the distributed geometric Koopman operator by exploiting the sparsity of the multi agent system is shown in lower right, with colors in the Koopman matrix capturing the distributed connection in the agent topology (white blocks correspond to no edges between the agents and hence they are all zeros).

61

62 **Contributions.** The main contributions of this paper are summarized as follows:

- 63 • We develop methods for learning distributed Koopman operator for large-scale networks, using
 64 system topology and network sparsity properties for NDS. We present a system theoretic learning
 65 approach that can exploit the network connectivity structure via GNNs.
- 66 • We introduce information theoretic-based clustering strategies for sparse NDS to learn a coars-
 67 ened structure and model the system using a hierarchical multi-agent paradigm.
- 68 • We present theoretical results on bounding the performance of the distributed geometric Koop-
 69 man operator with respect to its centralized counterpart.

- We demonstrate that DKGNN yields two benefits. It improves the scalability of learning, and for sparse NDS with divergent dynamics across different parts of the network, it outperforms prediction performance of centralized approaches.

1.1 Related Work

Koopman operator theory The infinite-dimensional Koopman operator is computationally intractable. Several methods for identifying approximations of the infinite-dimensional Koopman operator on a finite-dimensional space have recently been developed. Most notable works include dynamic mode decomposition (DMD) [17, 24], extended DMD (EDMD) [18, 25], Hankel DMD [26], naturally structured DMD (NS-DMD) [27] and deep learning based DMD (deepDMD) [20, 28]. These methods are data-driven and one or more of these methods have been successfully applied for system identification [17, 29] including system identification from noisy data [30], data-driven observability/controllability gramians for nonlinear systems [31, 32], control design [33–35], data-driven causal inference in dynamical systems [36] and to identify persistence of excitation conditions for nonlinear systems [37]. [38] discusses distributed design of Koopman without control and using dictionary lifting functions.

Graph Neural Networks GNNs [22, 39] have found widespread use into every application involving non-Euclidean data [40]. Extending GNNs to model physics-driven processes gives rise to a new class of physics-inspired neural networks (PINN) [8–10]. A common theme is to model many-body interactions via a nearest-neighbor graph and then model the evolution of that graph [6, 7, 9]. However, addressing issues around compositionality [7, 23] and scalability becomes important as the foundation for PI(G)NN matures and we seek to model larger, multi-scale spatio-temporal interactions. Moreover, applications such as molecular biology [20] and power grid [41] motivate the modeling of NDS where the graph structure is distinct from k-nearest neighbor graphs, with sparsity and connectivity that resemble small-world networks. Recent works such as [21] provides a bridge that seeks to integrate GNNs and Koopman operators to improve generalization ability and result in simpler linear transition dynamics. However, their approach for learning Koopman state transitions and GNN embedding results in performance and scalability bottlenecks when system size increases.

2 Methodology

2.1 Networked Dynamical Systems and the Koopman Operator

Problem Statement: Consider a networked dynamical system (NDS) evolving over a network, $\mathcal{G} = (\mathcal{V}, \mathcal{E})$. Let the number of nodes and edges be n_v and n_e respectively and the governing equation for the NDS on \mathcal{G} is given by,

$$x_{t+1} = F(x_t), \quad (1)$$

where $x_t \in \mathcal{M} \subseteq \mathbb{R}^n$ is the concatenated system state at time t and $F : \mathcal{M} \rightarrow \mathcal{M}$ is the discrete-time nonlinear transition mapping. Our goal is to learn the system dynamics as expressed in equation (1) in a distributed approach combining the Koopman operator theory, graph neural networks and by leveraging on network sparsity properties.

Exploring the network structure, the n_v nodes could be grouped to form n_a agents where $n_a \leq n_v$ and results in a network denoted by $\mathcal{G}_a = (\mathcal{V}_a, \mathcal{E}_a)$ with the state at any time t is partitioned as $x_t = [x_{t,1}^\top, \dots, x_{t,n_a}^\top]^\top$ where for every $\alpha \in \{1, \dots, n_a\}$, the states $x_{t,\alpha}$ belongs to agent α . For completion, we mention that the number of nodes in \mathcal{V}_a is equal to n_a . The motivation behind exploring the network structure is to develop models that will possess certain advantages when compared to the centrally learned models. A method to identify \mathcal{G}_a from \mathcal{G} for practical dynamical systems is discussed later in the paper. Associated with the system (1) is a linear operator, namely the Koopman operator \mathbb{U} [42] which is defined as follows.

Definition 1 (Koopman Operator (KO) [42]). *Given any $h \in L^2(\mathcal{M})$, the Koopman operator $\mathbb{U} : L^2(\mathcal{M}) \rightarrow L^2(\mathcal{M})$ for the system (1) is defined as $[\mathbb{U}h](x) = h(F(x))$, where $L^2(\mathcal{M})$ is the space of square integrable functions on \mathcal{M} .*

Originally developed for autonomous systems, recently Koopman framework has been extended to systems with control [43, 44]. In this paper we consider a controlled dynamical system of the form:

$$x_{t+1} = F(x_t) + G(x_t)u_t, \quad (2)$$

119 where $G : \mathcal{M} \rightarrow \mathbb{R}^{n \times q}$ is the input vector field and $u_t \in \mathbb{R}^q$ denote the control input to the system at
 120 time t . The Koopman operator associated with (2) is defined on an extended state-space obtained as
 121 the product of the original state-space and the space of all control sequences, resulting in a control-
 122 affine dynamical system on the extended state-space [43, 44]. In general, the Koopman operator is an
 123 infinite-dimensional operator, but for computation purposes, a finite-dimensional approximation of
 124 the operator is constructed from the obtained time-series data as discussed below.

125 Consider the time-series data from a networked dynamical system as $X = [x_1 \ x_2 \ \dots \ x_k] \in$
 126 $\mathbb{R}^{n \times k}$, and the corresponding control inputs $U = [u_1 \ u_2 \ \dots \ u_k] \in \mathbb{R}^{q \times k}$. Define one time-step
 127 separated datasets, X_p and X_f from X as $X_p = [x_1, x_2, \dots, x_{k-1}]$, $X_f = [x_2, x_3, \dots, x_k]$ and let
 128 $\mathcal{S} = \{\Psi_1, \dots, \Psi_m\}$ be the choice of non-linear functions or observables where $\Psi_i \in L^2(\mathbb{R}^n, \mathcal{B}, \mu)$
 129 (where \mathcal{B} is the Borel σ algebra and μ denote the measure [42]) and $\Psi_i : \mathbb{R}^n \rightarrow \mathbb{C}$. Define a vector
 130 valued observable function $\Psi : \mathbb{R}^n \rightarrow \mathbb{C}^m$ as, $\Psi(x) := [\Psi_1(x) \ \Psi_2(x) \ \dots \ \Psi_m(x)]^\top$. Then the
 131 following optimization problem which minimizes the least-squares cost yields the Koopman operator
 132 and the input matrix.

$$\min_{A,B} \|Y_f - AY_p - BU\|_F^2 \quad (3)$$

133 where $Y_p = \Psi(X_p) = [\Psi(x_1), \dots, \Psi(x_{k-1})]$, $Y_f = \Psi(X_f) = [\Psi(x_2), \dots, \Psi(x_k)]$, $A \in \mathbb{R}^{m \times m}$ is
 134 the finite dimensional approximation of the Koopman operator defined on the space of observables and
 135 the matrix $B \in \mathbb{R}^{m \times q}$ is the input matrix. The optimization problem (3) can be solved analytically
 136 and the approximate Koopman operator and the input matrix are given by $[A \ B] = Y_f[Y_p \ U]^\dagger$
 137 [43], where $(\cdot)^\dagger$ is the Moore-Penrose pseudo-inverse of a matrix. Identifying the observable functions
 138 such that \mathcal{S} is invariant under the action of the Koopman operator is challenging. In this work, graph
 139 neural network-based mappings are used to construct the non-linear observable functions that satisfy
 140 the invariance by simultaneously learning the observables and the Koopman operator.

141 2.2 Graph Neural Network based Koopman Observables

142 Consider the network \mathcal{G} with n_v nodes where the time-series data at each node is supplemented with
 143 the node attribute capturing the nature of the node, denoted by the vector x_{v_i} where $i = \{1, 2, \dots, n_v\}$.
 144 For instance, we can characterize the generators in a electric power grid network with their inertia
 145 values. Similarly, the designer can embed knowledge about the interaction between the agents using
 146 edge attributes, denoted as $x_{e_{ij}}$ for the edge connecting nodes i and j . We consider a graph neural
 147 network embedding to transition from the actual state-space to the lifted state-space using multiple
 148 compositional neural operations. At the t^{th} time-step, the node, and edge attributes are combined
 149 along with the state vectors of the agents which are compactly written as,

$$x_{t,i}^k = f_v^k(x_{t,i}^{k-1}, \sum_{j \in \mathcal{N}(i)} f_e^k(x_{t,i}^{k-1}, x_{v_i}^{k-1}, x_{t,j}^{k-1}, x_{v_j}^{k-1}, x_{e_{ij}}^{k-1})) \quad (4)$$

150 where the superscript k denotes the k^{th} layer of the GNN, and functions $f_e(\cdot)$, and $f_v(\cdot)$ are edge
 151 and node-level aggregation functions in a GNN architecture. We use $\phi(\cdot)$ to denote the multi-layer
 152 GNN operation in a compact form.

153 3 Distributed Geometric Koopman Operator with Control Inputs

154 This section formally presents the computation of distributed geometric Koopman operator with
 155 control. The (centralized) Koopman operator with control input for the system (2) is obtained by
 156 solving (3). For the n_a agent NDS, the resultant KO can be represented as n_a^2 block matrices:

$$A = \begin{bmatrix} A_1 \\ A_2 \\ \vdots \\ A_{n_a} \end{bmatrix} = \begin{bmatrix} A_{11} & A_{12} & \cdots & A_{1n_a} \\ A_{21} & A_{22} & \cdots & A_{2n_a} \\ \vdots & \vdots & \ddots & \vdots \\ A_{n_a 1} & A_{n_a 2} & \cdots & A_{n_a n_a} \end{bmatrix} \quad (5)$$

157 The dynamics of the α^{th} agent have the dimension, m_α , such that, $\sum_{\alpha=1}^{n_a} m_\alpha = m$. It now follows
 158 that the block matrix $A_{\alpha\beta} \in \mathbb{R}^{m_\alpha \times m_\beta}$ denotes the transition of agent α with respect to β and the
 159 transition mapping for agent α is given by A_α . Similarly, the control input matrix is partitioned

160 as $B = \text{blkdiag}(B_1, B_2, \dots, B_{n_a})$, where the matrix B_α corresponds to input matrix of agent
 161 $\alpha \in \{1, 2, \dots, n_a\}$. The objective of the distributed learning is to compute these block matrices in
 162 a distributed manner and form the geometric Koopman operator and the control input matrix for
 163 the complete NDS as opposed to directly solving the centralized optimization problem in Eq. (3)
 164 without sacrificing the performance with the distributed method. There are two major advantages
 165 to this approach. Firstly, if there is change in the local agent behavior, one can simply update the
 166 transition mapping corresponding to that agent and the agents dependent on it to learn the full system
 167 evolution. Secondly, computational advantages can be obtained by incorporating parallel learning of
 168 each agent transition mapping and this approach is more appropriate for the sparse networks.

169 By exploiting the topology of the network, the KO and the control input matrices are computed
 170 in a distributed manner. As a consequence, if agent i is not a neighbor of agent j , that is, the
 171 dynamics of agent i is not affected by the dynamics of agent j , we make $A_{ij} = 0$. Therefore, for
 172 every $\alpha \in \{1, 2, \dots, n_a\}$, let \hat{A}_α be the transition mapping corresponding to the agent α , then
 173 the distributed Koopman is given by $A_D = [\hat{A}_1^\top \ \hat{A}_2^\top \ \dots \ \hat{A}_{n_a}^\top]^\top$. For a sparse network, the
 174 distributed Koopman will be a sparse matrix irrespective of the centralized Koopman being either
 175 sparse or full (Figure 1). Consider X_p and X_f be the one time-step separated time-series data on the
 176 state space, ϕ be the GNN-embedding that maps the state space data into an embedded space. Then
 177 the time-series data on the embedded space for every agent can be expressed in terms of the neighbor
 178 and non-neighbor agents.

179 **Remark 2.** The one time-step forwarded time-series data corresponding to agent α is given by
 180 $A_\alpha Y_p = [A_{\mathcal{N}(\alpha)} \ A_{\overline{\mathcal{N}(\alpha)}}] \begin{bmatrix} Y_{p, \mathcal{N}(\alpha)} \\ Y_{p, \overline{\mathcal{N}(\alpha)}} \end{bmatrix}$, where $\mathcal{N}(\alpha)$ is the set of agents containing the neighbors of
 181 agent α and itself, $\overline{\mathcal{N}(\alpha)}$ is the set of agents who are non-neighbors of agent α and the (rectangular)
 182 matrices, $A_{\mathcal{N}(\alpha)}$ and $A_{\overline{\mathcal{N}(\alpha)}}$ are the transition mappings associated with the agent α .

183 Let $R_{p,\alpha}$, $R_{f,\alpha}$, and $R_{u,\alpha}$ be the transformation matrices defined in such a way that they remove zero
 184 rows of any matrix, D when pre-multiplied to the matrix, D . Suppose if the matrix D has no zero
 185 rows then the transformation matrices are identity.

186 **Theorem 3.** The centralized Koopman (A, B) learning problem described in Eq. (3) can be
 187 expressed as a distributed Koopman (A_D, B_D) learning problem such that there exists ma-
 188 trices, $\hat{A}_1, \hat{A}_2, \dots, \hat{A}_{n_a}$, $\hat{B}_1, \hat{B}_2, \dots, \hat{B}_{n_a}$ and the distributed Koopman operator is given by
 189 $A_D = [\hat{A}_1^\top \ \hat{A}_2^\top \ \dots \ \hat{A}_{n_a}^\top]^\top$, input matrix is $B_D = \text{blkdiag}(\hat{B}_1, \hat{B}_2, \dots, \hat{B}_{n_a})$ where for
 190 $\alpha \in \{1, 2, \dots, n_a\}$, $\hat{A}_\alpha = A_{\mathcal{N}(\alpha)} R_{p,\alpha}$, $\hat{B}_\alpha = B_\alpha R_{u,\alpha}$ and $A_{\mathcal{N}(\alpha)}, B_\alpha$ are obtained as a solu-
 191 tion to the optimization problem $\min_{A_{\mathcal{N}(\alpha)}, B_\alpha} \|Y_{f,\alpha} - A_{\mathcal{N}(\alpha)} Y_{p,\mathcal{N}(\alpha)} - B_\alpha U_\alpha\|_F^2$.

192 From Theorem 3, with $g_t = \phi(x_t)$, ϕ being the GNN encoder, the distributed geometric Koopman
 193 operator system with control input is given by $g_{t+1} = A_D g_t + B_D u_t$.

194 **Corollary 4.** The distributed learning problem and the centralized learning problem yield the same
 195 Koopman operator for a fully connected network.

196 The proofs for Theorem 3 and Corollary 4 are included in the appendix.

197 3.1 Training Distributed Geometric Koopman Model

198 The state space data is
 199 mapped to the GNN-
 200 embedded space using the
 201 GNN encoder ϕ . To
 202 retrieve the actual state
 203 space data from the GNN-
 204 embedded space, we use
 205 a decoding GNN opera-
 206 tor such that, $\hat{x}_t = \varphi(g_t)$.
 207 The decoder $\varphi(\cdot)$ fol-
 208 lows similar GNN archi-
 209 tecture as encoder how-
 210 ever it maps from the

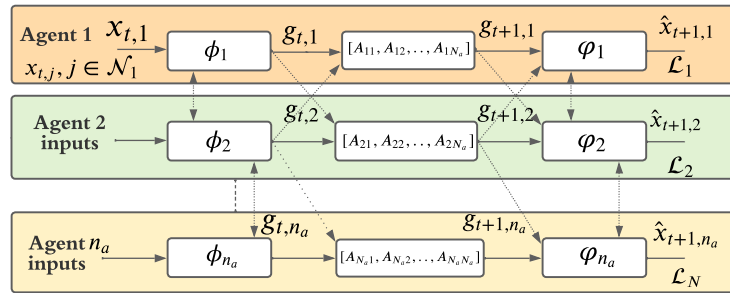


Figure 2: Distributed geometric Koopman architecture

211 lifted Koopman space to the original state space. Looking into the agent-wise architectural de-
 212 tail, both encoder and decoder functions can be represented for the i^{th} agent as $\phi_i(\cdot), \varphi_i(\cdot)$ as shown
 213 in Figure 2 with the understanding that all the GNN functionalities take the neighbouring agent
 214 states and attributes as additional inputs. This facilitates the computation of Koopman matrices in a
 215 distributed manner. This architecture leads us to compute an auto-encoding loss, and a prediction
 216 loss over the time-steps $t = 1, 2, \dots, k - 1$, and are given as follows:

$$\mathcal{L}_{ae} = \frac{1}{k} \sum_{t=1}^{k-1} \sum_{i=1}^{n_a} \varphi_i(\phi_i(x_{t,i})) - x_{t,i}, \quad \mathcal{L}_p = \frac{1}{k} \sum_{t=1}^{k-1} \sum_{i=1}^{n_a} \varphi_i(g_{t+1,i}) - x_{t+1,i},$$

217 with total loss of $\mathcal{L} = \mathcal{L}_{ae} + \mathcal{L}_p$. The algorithm will consist of two main update steps sequentially,
 218 one to update the Koopman and the control input matrix in a distributed manner for a fixed set
 219 of GNN encoder and decoder parameters, and another to update GNN weights with a learned
 220 distributed geometric Koopman representation. Algorithm 1 shows the computational steps where
 221 the function `DistributedKoopmanMatrices(\cdot)` presents the distributed Koopman state and input
 222 matrices, A_D, B_D . Thereafter the `Main(\cdot)` function runs the update of the distributed Koopman
 223 matrices and the GNN parameters sequentially for each epoch as shown in steps 15 and 16. For
 224 simplicity of representation in the algorithm, we use the compact notations $\phi(\cdot)$ and $\varphi(\cdot)$ instead of
 225 agent-wise representation as in Figure 2.

Algorithm 1 Distributed Geometric Koopman Operator with Control Computation

```

1: function DISTRIBUTEDKOOPMANMATRICES( $X_p, X_f, U, \phi$ )
2:   Map the time-series data to the GNN-embedded space using  $\phi$  as follows:
        $Y_p = \phi(X_p) = [\phi(x_1), \phi(x_2), \dots, \phi(x_{k-1})], Y_f = \phi(X_f) = [\phi(x_2), \phi(x_3), \dots, \phi(x_k)]$ 
3:   for  $\alpha = 1, 2, \dots, n_a$  do
4:     Define the transformation matrices for agent  $\alpha$  as:
            $T_{p,\alpha} := \text{blkdiag}(ae_1, \dots, ae_{n_a}), T_{f,\alpha} := \text{blkdiag}(ee_1, \dots, ee_{n_a}),$ 
            $T_{u,\alpha} := \text{blkdiag}(eu_1, \dots, eu_{n_a}),$  where
            $ae_i = (a_\alpha + e_\alpha)_i \otimes I_{m_i}, ee_i = (e_\alpha)_i \otimes I_{m_i}, eu_i = (e_\alpha)_i \otimes I_{q_i},$ 
       where  $\otimes$  is the Kronecker product.
5:     Compute  $Y_{f,\alpha}, Y_{p,\mathcal{N}(\alpha)}, U_\alpha$  associated with agent  $\alpha$  as
            $Y_{f,\alpha} = R_{f,\alpha} T_{f,\alpha} Y_f, Y_{p,\mathcal{N}(\alpha)} = R_{p,\alpha} T_{p,\alpha} Y_p, U_\alpha = R_{u,\alpha} T_{u,\alpha} U$ 
6:     Solve the optimization problem:  $\min_{A_{\mathcal{N}(\alpha)}, B_\alpha} \|Y_{f,\alpha} - A_{\mathcal{N}(\alpha)} Y_{p,\mathcal{N}(\alpha)} - B_\alpha U_\alpha\|_F^2$ 
7:     Compute  $\hat{A}_\alpha = A_{\mathcal{N}(\alpha)} R_{p,\alpha}$  and  $\hat{B}_\alpha = B_\alpha R_{u,\alpha}$ 
8:   end for
9:   return:  $A_D = [\hat{A}_1^\top \quad \hat{A}_2^\top \quad \dots \quad \hat{A}_n^\top]^\top, B_D = \text{blkdiag}(\hat{B}_1, \hat{B}_2, \dots, \hat{B}_n).$ 
10: end function
11: function MAIN()
12:   Given state ( $X_p, X_f$ ) and input ( $U$ ) time-series data from a  $N_a$  agent network
13:   Initialize the GNN-based encoder ( $\phi$ ) and decoder ( $\varphi$ ) network
14:   for epochs =  $1, 2, \dots, N_{\text{epoch}}$  do
15:     Koopman Update: Run  $(A_D, B_D) = \text{DistributedKoopmanMatrices}(X_p, X_f, U, \phi)$ 
16:     GNN Update: Compute  $\mathcal{L} = \mathcal{L}_p + \mathcal{L}_{ae}$ , and backpropagate  $\mathcal{L}$  to update  $\phi, \varphi$  parameters.
17:   end for
18:   return: Updated  $A_D, B_D, \phi$ , and,  $\varphi$ .
19: end function
    
```

226 3.2 Multi-Agent Network Construction via Information Transfer-based Clustering

227 Mapping of nodes in an NDS to nodes in an agent network is a core aspect for our proposed method.
 228 We use an information-theoretic clustering method [45] that exploits both the adjacency matrix
 229 structure as well as dynamical properties of the network for this task. For a dynamical system, the
 230 definition of information transfer [46] from a dynamical state $x_{t,i}$ to another state $x_{t,j}$ is based on
 231 the intuition that the total entropy of a dynamical state $x_{t,j}$ is equal to the sum of the entropy of $x_{t,j}$
 232 when another state $x_{t,i}$ is not present in the dynamics and the amount of entropy transferred from $x_{t,i}$

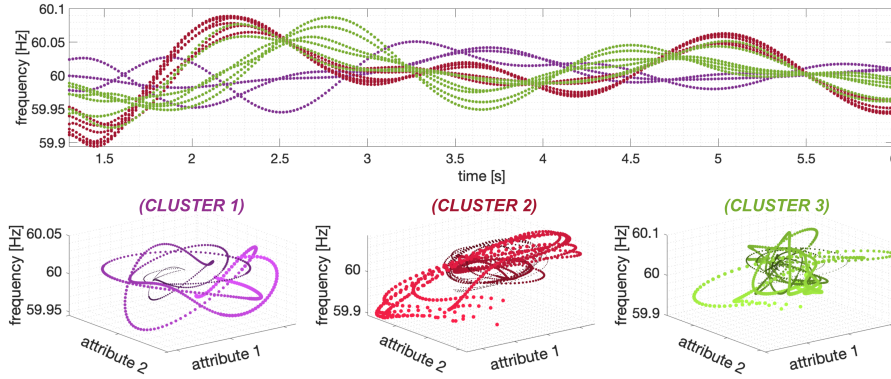


Figure 3: Illustration of divergent cluster dynamics from a power network. Top plot shows that the transient frequency trajectories from three different clusters behave differently. Phase-space plots in the bottom row illustrate the temporal evolution of the nodal attributes in each cluster, initial time-points are marked larger and lighter, while later time-points are marked thinner and darker.

233 to $x_{t,j}$. In particular, for a discrete-time dynamical system $x_{t+1} = F(x_t)$, where $x_t = [x_{t,1}^\top \ x_{t,2}^\top]^\top$
 234 and $F = [f_1^\top \ f_2^\top]^\top$, the one-step information transfer from $x_{t,1}$ to $x_{t,2}$, as the system evolves from
 235 time-step t to $t + 1$ is $[T_{x_{t,1} \rightarrow x_{t,2}}]^{t+1} = H(x_{t+1,2}|x_{t,2}) - H_{\neq t,1}(x_{t+1,2}|x_{t,2})$. Here, $H(x_{t+1,2}|x_{t,2})$
 236 is the conditional Shannon entropy of $x_{t,2}$ for the original system and $H_{\neq t,1}(x_{t+1,2}|x_{t,2})$ is the
 237 conditional entropy of $x_{t,2}$ for the system where $x_{t,1}$ has been held frozen from at time t . Note that
 238 the information transfer is in general asymmetric and characterize the influence of one state on any
 239 other state. Furthermore, for stable dynamical system the information transfer between the states
 240 always settle to a steady state value.

241 We use this information transfer measure to define an influence graph for the NDS studied in this paper.
 242 We form a directed weighted graph with the states as the nodes and introduce an edge from $x_{t,1}$ to
 243 $x_{t,2}$ iff the information transfer from $x_{t,1}$ to $x_{t,2}$ is non-zero. Moreover, the edge-weight for the edge
 244 $x_{t,1} \rightarrow x_{t,2}$ is $\exp(-|T_{x_{t,1} \rightarrow x_{t,2}}|/\beta)$ [45], where $|T_{x_{t,1} \rightarrow x_{t,2}}|$ is the steady-state information transfer
 245 from $x_{t,1}$ to $x_{t,2}$ (we assume stable dynamics) and $\beta > 0$ is a parameter similar to temperature in a
 246 Gibbs' distribution. Applying this to a dynamical system, a directed weighted graph is computed
 247 based on the information transfer and is clustered accordingly to obtain a multi-agent network.
 248 Figure 3 uses a power network example to illustrate how the nodal attributes from different clusters
 249 demonstrate different transient evolution trajectories.

250 4 Numerical Experiments

251 In this section, we aim to answer the following research questions through our experiments: **(RQ1)**
 252 How does the distributed GNN-based Koopman (DKGNN) model's performance compare with
 253 other state-of-the-art approaches such as centralized GNN-based Koopman (CKGNN) [21] and
 254 graph neural network approaches for modeling multi-body interactions [47] **(RQ2)** How do various
 255 dynamical system properties such as sparsity, spatio-temporal correlation, and damping properties
 256 influence the performance boost from the distributed algorithm? **(RQ3)** What is the potential for
 257 distributed approaches for scaling to larger NDS in the future?

Power Grid	CKGNN	DKGNN area-wise clustering	DKGNN IT-based clustering	PN	Oscillator	CKGNN	DKGNN	PN
Disturbance Location	MSE	MSE	MSE	MSE	Disturbance Location	MSE	MSE	MSE
One hop	0.0352	0.0064	0.0079	0.1123	High damping	1.938E-04	1.026E-04	3.6E-04
Two hops	0.0212	0.0044	0.0049	0.2498	Low Damping	1.404E-04	1.185E-04	5.205E-04
Three hops	0.029	0.0075	0.0098	0.0468	Random	4.86E-05	4.059E-04	4.7328
High degree	0.0055	0.0013	8.538E-04	0.0246				
Low degree	0.0195	0.005	0.006	0.0427	Rope	0.2301	0.2008	0.3091

Table 1: Prediction performance of the proposed distributed geometric Koopman approach with other baselines in terms of mean square errors (MSE) averaged over all time-steps and states for test trajectories.

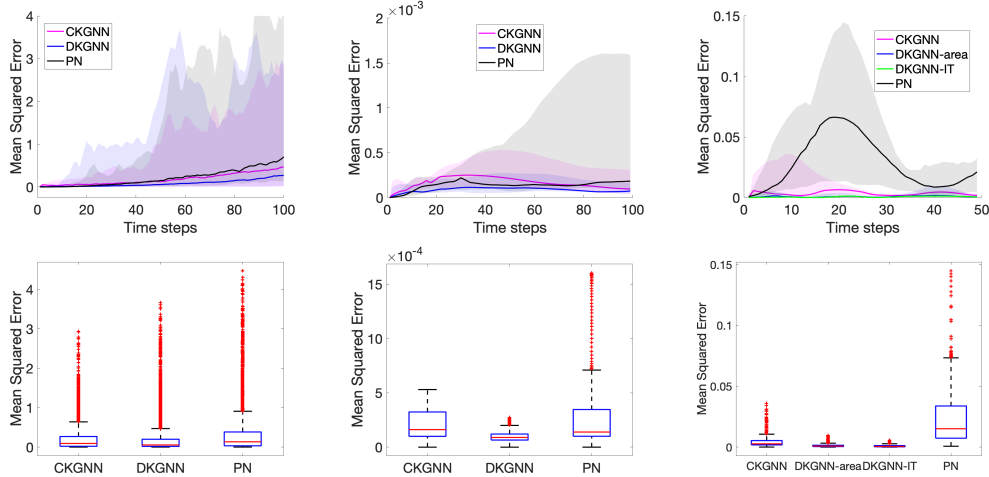


Figure 4: DKGNN out-performs the baselines. Columns A, B, C represent for rope, oscillator (high damping) and grid (high degree) examples, respectively. Prediction error over time-steps with darker lines representing median are shown in Row A, and MSE-based box plots are shown in Row B.

258 **Environments.** We perform numerical experiments on three different data-sets. The baseline rope
 259 system introduced in [7] consists of a set of six objects connected via a line graph. The second dataset
 260 is a network of oscillators which is a prototype used for modelling various real-world systems in
 261 biology [48, 49], synchronization of fireflies [50], superconducting Josephson junctions [51] etc. We
 262 consider a sparse network of oscillators consisting of 50 agents where the dynamics at each oscillator
 263 are governed by a second-order swing differential equation. The network density for this network
 264 is 0.0408. Our third dataset studies a significantly larger and complex system of immense practical
 265 importance. Power grid networks [52] are complex infrastructures that are essential for every aspect
 266 of modern life. The ability to predict transient behavior in such networks is key to the prevention
 267 of cascading failures and effective integration of renewable energy sources [53, 54]. We consider
 268 the IEEE 68-bus power grid model [55] that represents the interconnections of New England Test
 269 System and New York Power System. This is a sparse, heterogeneous network with a network density
 270 0.0378; the network has 68-nodes, with 16-nodes representing generators and the rest being loads.
 271 The ability to accurately predict changes in voltage and frequency is key to capturing the tendency
 272 of a power grid to move towards undesired oscillatory regions. Transient stability simulations for
 273 the grid datasets are performed by the Power Systems Toolbox [56]. We provide more details on the
 274 datasets and experiments in the supplementary.

275 **Baselines and Implementation Details.** We baseline our method against centralized GNN-based
 276 Koopman (CKGNN) [21] and propagation network (PN), a GNN-based approach [47] using their
 277 available implementations. We evaluate all models on the trajectory prediction task where we predict
 278 the node-level time-series measurements for each of these environments that represent velocity of
 279 objects (rope), angles and frequencies of oscillators, and frequency measurements for the power grid.
 280 For PN, we slightly modify the prediction workflow from the author-provided implementation to
 281 make sure that we always feed the PN with the predicted signal values except for the initial signal
 282 input for the prediction task in consecutive time steps. Our methods are implemented on the Pytorch
 283 framework [57] and run on an NVIDIA A100 GPU. For PN baseline, we used 3 propagation steps
 284 with 32 as the batch size. The dimensions of the hidden layer of relation encoder, object encoder,
 285 and propagation effect are set as follows, for PN we use 150, 100, and 100, respectively for all the
 286 cases, for the rope system with CKGNN and DKGNN, we have used 120, 100, and 100, and for the
 287 oscillator and grid example with both CKGNN and DKGNN, these are set to be 60. The models
 288 are trained with Adam based stochastic gradient descent optimizer with a learning rate of 10^{-5} . For
 289 rope, we consider 10,000 episodes with 100 time-steps and training-testing division of 90% – 10%,
 290 and batch size of 8 episodes. We consider the oscillator node state trajectories of 100 time-steps
 291 and trained with a total of 9000 time-steps, batch size of 10 trajectories, and have tested with three
 292 different testing configurations and predicting for each trajectory of 100 time-steps. Considering the
 293 power grid network, we have considered 50 time-steps to capture the initial fast transients and train
 294 the model with 1100 time steps with a batch size of 5 episodes along with testing in five different
 295 scenarios with multiple testing trajectories each with 50 time steps.

296 **RQ1: Prediction performance analysis.** Figure 4 shows that DKGNN outperforms other baselines
 297 in trajectory prediction. Table 1 reports the mean square error (MSE) averaged over all time-
 298 steps and over all states in the test trajectory dataset. The rope system is minimally sparse with
 299 a network density of 0.33, thereby resulting in improved predictive performance for the DKGNN
 300 when compared to KGNN. The improvements are significantly pronounced for sparser and larger
 301 network models of oscillators (network density 0.0408) and power grid (network density 0.0378).
 302 The superior prediction performance over considerable trajectory time-steps (as demonstrated in
 303 Figure 4 second row) substantiates the applicability of DKGNN for sparse NDS.

304 **RQ2.1 Performance with respect to varying NDS properties.** The damping parameter provides
 305 us with a way to systematically study the response of an NDS to an input. Lower damping implies
 306 that the system will take longer to converge to a steady state. We hypothesize that the introduction of
 307 input perturbations of the same magnitude at different nodes will evoke different responses depending
 308 on the connectivity structure around these nodes. For the oscillator network, we consider testing
 309 scenarios with disturbances created at high damping nodes (> 13 in appropriate units) and low
 310 damping nodes (< 1). We consider five different configurations for the power grid network. Three of
 311 the scenarios are based on the perturbations in the loads which are respectively one-hop, two-hop, and
 312 three-hop away from the generator buses, and two other load disturbance scenarios are considered at
 313 locations with high and low degrees of connectivity. We observe DKGNN approach is able to produce
 314 better prediction performance with all of these scenarios (81, 79, 74, 76, 74% improvements with
 315 area-wise partitioning, and 77, 76, 66, 84, 69% improvements with information-theoretic partitioning
 316 for the five cases listed in Table I from top to bottom with respect to the centralized approach).
 317 The second and third columns of Figure 4 correspond to the oscillator (where the disturbance is at
 318 high-damping nodes), and the power grid (where the disturbance is at high-degree buses), respectively,
 319 where both of them show the superior performance of DKGNN to the baselines.

320 **RQ2.2 Performance with respect to sparse NDS clustering.** This subsection reports our validation
 321 of the effectiveness of the information-theoretic clustering based agent structure discovery using the
 322 power grid network. The IEEE-68 bus grid network specifications also include an area-wise parti-
 323 tioning that is done based on eigenvalue separation and extensive application of domain-knowledge
 324 [58]. Both the expert-driven partitioning and our clustering driven partitioning divide the grid into 5
 325 clusters and yields a 5-agent network to use for the training. Table I and Figure 4 show that DKGNN
 326 exploits the localized dominant dynamics and yields superior predictive performance when compared
 327 to the centralized approaches such as CKGNN and PN.

328 **RQ3. Computational Scalability.** We compare the run time of our DKGNN with the
 329 corresponding centralized one, KGNN. Let $\tau(\phi + A_D + \varphi)$ denote the combined compu-
 330 tation time for GNN encoder (ϕ), distributed Koopman (A_D) and the GNN decoder (φ).
 331 Similarly, $\tau(\phi + A + \varphi)$ denote the computation for KGNN where the centralized Koopman (A) is obtained.
 332 The reduction in total run-time (%) is computed as $\frac{\tau(KGNN) - \tau(DKGNN)}{\tau(KGNN)} \times 100$. From Figure 5, it is clear
 333 there is a significant reduction in run time for the larger
 334 and sparser networks of oscillator (50 nodes with network
 335 density = 0.041), and power grid (68 nodes, 5 clustered
 336 areas and network density of 0.038). These examples see
 337 a considerable performance boost (45.63% for oscillator
 338 and 32% for power grid) owing to capturing the dominant
 339 localized dynamic behavior. The rope which is a
 340 smaller system with 6 nodes and single excitation (at the
 341 top) shows only slightly improvement in runtime (5%), owing to high network density (0.33).
 342
 343

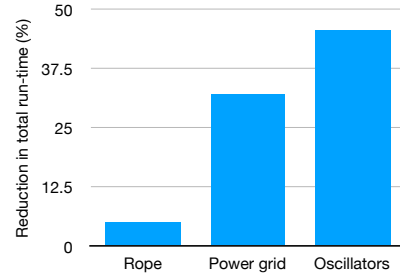


Figure 5: Scalability of DKGNN compared to KGNN model.

344 5 Conclusions

345 We present a geometric deep learning based distributed Koopman operator (DKGNN) framework
 346 that can exploit dynamical system sparsity to improve computational scalability. Our results on
 347 bounding the DKGNN performance with respect to its centralized counterpart provides a rigorous
 348 theoretical foundation. Extensive empirical studies on large NDS of oscillators and practical power
 349 grid models show the effectiveness of DKGNN design with respect to varying degree of NDS
 350 dynamical properties and sparsity patterns. Future research will look into incorporating attention
 351 capability to the distributed design, investigating the robustness aspects in presence of physical or
 352 adversarial faults, and perform control designs on the learned distributed dynamical model.

References

- 353
- 354 [1] Coryn AL Bailer-Jones, David JC MacKay, and Philip J Withers. A recurrent neural network
355 for modelling dynamical systems. *Network: Computation in Neural Systems*, 9(4):531–547,
356 1998. 1
- 357 [2] Min Han, Zhiwei Shi, and Wei Wang. Modeling dynamic system by recurrent neural network
358 with state variables. In *International Symposium on Neural Networks*, pages 200–205. Springer,
359 2004.
- 360 [3] Olalekan Ogunmolu, Xuejun Gu, Steve Jiang, and Nicholas Gans. Nonlinear systems identifica-
361 tion using deep dynamic neural networks. *arXiv preprint arXiv:1610.01439*, 2016.
- 362 [4] Yu Wang. A new concept using LSTM neural networks for dynamic system identification. In
363 *2017 American Control Conference (ACC)*, pages 5324–5329. IEEE, 2017.
- 364 [5] FA Gers, J Schmidhuber, and F Cummins. Learning to forget: Continual prediction with lstm.
365 *Neural computation*, 12(10):2451–2471, 2000. 1
- 366 [6] Peter Battaglia, Razvan Pascanu, Matthew Lai, Danilo Jimenez Rezende, et al. Interaction
367 networks for learning about objects, relations and physics. In *Advances in neural information*
368 *processing systems*, pages 4502–4510, 2016. 1, 2, 3
- 369 [7] Yunzhu Li, Jiajun Wu, Russ Tedrake, Joshua B Tenenbaum, and Antonio Torralba. Learning
370 particle dynamics for manipulating rigid bodies, deformable objects, and fluids. *arXiv preprint*
371 *arXiv:1810.01566*, 2018. 2, 3, 8
- 372 [8] Maziar Raissi, Paris Perdikaris, and George E Karniadakis. Physics-informed neural networks:
373 A deep learning framework for solving forward and inverse problems involving nonlinear partial
374 differential equations. *Journal of Computational physics*, 2019. 3
- 375 [9] Alvaro Sanchez-Gonzalez, Jonathan Godwin, Tobias Pfaff, Rex Ying, Jure Leskovec, and
376 Peter W Battaglia. Learning to simulate complex physics with graph networks. *arXiv preprint*
377 *arXiv:2002.09405*, 2020. 2, 3
- 378 [10] Martin JA Schuetz, J Kyle Brubaker, and Helmut G Katzgraber. Combinatorial optimization
379 with physics-inspired graph neural networks. *Nature Machine Intelligence*, 4(4):367–377, 2022.
380 1, 3
- 381 [11] Tohru Katayama. *Subspace methods for system identification*. Springer Science & Business
382 Media, 2006. 1
- 383 [12] Michel Verhaegen and Vincent Verdult. *Filtering and system identification: a least squares*
384 *approach*. Cambridge University Press, 2007.
- 385 [13] Rik Pintelon and Johan Schoukens. *System identification: a frequency domain approach*. John
386 Wiley & Sons, 2012.
- 387 [14] Zoltán Szabó, Peter SC Heuberger, József Bokor, and Paul MJ Van den Hof. Extended Ho-
388 Kalman algorithm for systems represented in generalized orthonormal bases. *Automatica*, 36
389 (12):1809–1818, 2000. 1
- 390 [15] Bernard O Koopman. Hamiltonian systems and transformation in Hilbert space. *Proceedings of*
391 *the National Academy of Sciences of the United States of America*, 17(5):315, 1931. 1
- 392 [16] Igor Mezić. Spectral properties of dynamical systems, model reduction and decompositions.
393 *Nonlinear Dynamics*, 41(1):309–325, 2005. 1
- 394 [17] Clarence W Rowley, Igor Mezic, Shervin Bagheri, Philipp Schlatter, Dans Henningson, et al.
395 Spectral analysis of nonlinear flows. *Journal of Fluid Mechanics*, 641(1):115–127, 2009. 1, 3
- 396 [18] Matthew O Williams, Ioannis G Kevrekidis, and Clarence W Rowley. A data-driven approxima-
397 tion of the Koopman operator: Extending dynamic mode decomposition. *Journal of Nonlinear*
398 *Science*, 25(6):1307–1346, 2015. 1, 3
- 399 [19] Bethany Lusch, J Nathan Kutz, and Steven L Brunton. Deep learning for universal linear
400 embeddings of nonlinear dynamics. *Nature communications*, 9(1):1–10, 2018. 1

- 401 [20] Enoch Yeung, Soumya Kundu, and Nathan Hodas. Learning deep neural network representations
402 for koopman operators of nonlinear dynamical systems. In *2019 American Control Conference*
403 (*ACC*), pages 4832–4839. IEEE, 2019. 1, 3
- 404 [21] Yunzhu Li, Hao He, Jiajun Wu, Dina Katabi, and Antonio Torralba. Learning compositional
405 koopman operators for model-based control. *arXiv preprint arXiv:1910.08264*, 2019. 2, 3, 7, 8,
406 14
- 407 [22] Franco Scarselli, Marco Gori, Ah Chung Tsoi, Markus Hagenbuchner, and Gabriele Monfardini.
408 The graph neural network model. *IEEE Transactions on Neural Networks*, 20(1):61–80, 2008.
409 2, 3
- 410 [23] Damian Mrowca, Chengxu Zhuang, Elias Wang, Nick Haber, Li Fei-Fei, Joshua B Tenenbaum,
411 and Daniel LK Yamins. Flexible neural representation for physics prediction. *arXiv preprint*
412 *arXiv:1806.08047*, 2018. 2, 3
- 413 [24] J Nathan Kutz, Steven L Brunton, Bingni W Brunton, and Joshua L Proctor. *Dynamic mode*
414 *decomposition: data-driven modeling of complex systems*. SIAM, 2016. 3
- 415 [25] Qianxiao Li, Felix Dietrich, Erik M Bollt, and Ioannis G Kevrekidis. Extended dynamic mode
416 decomposition with dictionary learning: A data-driven adaptive spectral decomposition of the
417 Koopman operator. *Chaos: An Interdisciplinary Journal of Nonlinear Science*, 27(10):103111,
418 2017. 3
- 419 [26] Hassan Arbabi and Igor Mezic. Ergodic theory, dynamic mode decomposition, and computation
420 of spectral properties of the Koopman operator. *SIAM Journal on Applied Dynamical Systems*,
421 16(4):2096–2126, 2017. 3
- 422 [27] Bowen Huang and Umesh Vaidya. Data-driven approximation of transfer operators: Naturally
423 structured dynamic mode decomposition. In *2018 Annual American Control Conference (ACC)*,
424 pages 5659–5664. IEEE, 2018. 3
- 425 [28] Naoya Takeishi, Yoshinobu Kawahara, and Takehisa Yairi. Learning Koopman invariant
426 subspaces for dynamic mode decomposition. In *Advances in Neural Information Processing*
427 *Systems*, pages 1130–1140, 2017. 3
- 428 [29] Peter J Schmid. Dynamic mode decomposition of numerical and experimental data. *Journal of*
429 *fluid mechanics*, 656:5–28, 2010. 3
- 430 [30] Subhrajit Sinha, Bowen Huang, and Umesh Vaidya. On robust computation of koopman operator
431 and prediction in random dynamical systems. *Journal of Nonlinear Science*, pages 1–34, 2019.
432 3
- 433 [31] Umesh Vaidya. Observability gramian for nonlinear systems. In *Decision and Control, 2007*
434 *46th IEEE Conference on*, pages 3357–3362. IEEE, 2007. 3
- 435 [32] Amit Surana and Andrzej Banaszuk. Linear observer synthesis for nonlinear systems using
436 Koopman operator framework. *IFAC-PapersOnLine*, 49(18):716–723, 2016. 3
- 437 [33] Steven L Brunton, Bingni W Brunton, Joshua L Proctor, and J Nathan Kutz. Koopman invariant
438 subspaces and finite linear representations of nonlinear dynamical systems for control. *PLoS*
439 *one*, 11(2):e0150171, 2016. 3
- 440 [34] Bowen Huang, Xu Ma, and Umesh Vaidya. Feedback stabilization using koopman operator. In
441 *2018 IEEE Conference on Decision and Control (CDC)*, pages 6434–6439. IEEE, 2018.
- 442 [35] Milan Korda and Igor Mezić. Koopman model predictive control of nonlinear dynamical
443 systems. In *The Koopman Operator in Systems and Control*, pages 235–255. Springer, 2020. 3
- 444 [36] S Sinha and U Vaidya. On data-driven computation of information transfer for causal inference
445 in discrete-time dynamical systems. *Journal of Nonlinear Science*, pages 1–26, 2020. 3
- 446 [37] Nibodh Boddupalli, Aqib Hasnain, Sai Pushpak Nandanoori, and Enoch Yeung. Koopman
447 operators for generalized persistence of excitation conditions for nonlinear systems. In *2019*
448 *IEEE 58th Conference on Decision and Control (CDC)*, pages 8106–8111. IEEE, 2019. 3
- 449 [38] Sai Pushpak Nandanoori, Seemita Pal, Subhrajit Sinha, Soumya Kundu, Khushbu Agarwal,
450 and Sutanay Choudhury. Data-driven distributed learning of multi-agent systems: A koopman
451 operator approach. In *2021 60th IEEE Conference on Decision and Control (CDC)*, pages
452 5059–5066. IEEE, 2021. 3

- 453 [39] Mostafa Haghir Chehreghani. Half a decade of graph convolutional networks. *Nature Machine*
454 *Intelligence*, 4(3):192–193, 2022. 3
- 455 [40] Michael M Bronstein, Joan Bruna, Yann LeCun, Arthur Szlam, and Pierre Vandergheynst.
456 Geometric deep learning: going beyond euclidean data. *IEEE Signal Processing Magazine*,
457 2017. 3
- 458 [41] Wenlong Liao, Birgitte Bak-Jensen, Jayakrishnan Radhakrishna Pillai, Yuelong Wang, and
459 Yusen Wang. A review of graph neural networks and their applications in power systems.
460 *Journal of Modern Power Systems and Clean Energy*, 2021. 3
- 461 [42] Andrzej Lasota and Michael C Mackey. *Chaos, fractals, and noise: stochastic aspects of*
462 *dynamics*, volume 97. Springer Science & Business Media, 2013. 3, 4
- 463 [43] Milan Korda and Igor Mezić. Linear predictors for nonlinear dynamical systems: Koopman
464 operator meets model predictive control. *Automatica*, 93:149–160, 2018. 3, 4
- 465 [44] Joshua L Proctor, Steven L Brunton, and J Nathan Kutz. Dynamic mode decomposition with
466 control. *SIAM Journal on Applied Dynamical Systems*, 15(1):142–161, 2016. 3, 4
- 467 [45] Subhrajit Sinha. Data-driven influence based clustering of dynamical systems.
468 *arXiv:2204.02373*, accepted for publication in European Control Conference, 2022. 6, 7
- 469 [46] Subhrajit Sinha and Umesh Vaidya. Causality preserving information transfer measure for
470 control dynamical system. In *2016 IEEE 55th Conference on Decision and Control (CDC)*,
471 pages 7329–7334. IEEE, 2016. 6
- 472 [47] Yunzhu Li, Jiajun Wu, Jun-Yan Zhu, Joshua B Tenenbaum, Antonio Torralba, and Russ Tedrake.
473 Propagation networks for model-based control under partial observation. pages 1205–1211,
474 2019. 7, 8
- 475 [48] Charles S Peskin. Mathematical aspects of heart physiology. *Courant Inst. Math*, 1975. 8
- 476 [49] Michael B Elowitz and Stanislas Leibler. A synthetic oscillatory network of transcriptional
477 regulators. *Nature*, 403(6767):335–338, 2000. 8
- 478 [50] John Buck. Synchronous rhythmic flashing of fireflies. ii. *The Quarterly review of biology*, 63
479 (3):265–289, 1988. 8
- 480 [51] Kurt Wiesenfeld, Pere Colet, and Steven H Strogatz. Synchronization transitions in a disordered
481 josephson series array. *Physical review letters*, 76(3):404, 1996. 8
- 482 [52] Florian Dörfler, Michael Chertkov, and Francesco Bullo. Synchronization in complex oscillator
483 networks and smart grids. *Proceedings of the National Academy of Sciences*, 110(6):2005–2010,
484 2013. 8
- 485 [53] Benjamin Schäfer, Dirk Witthaut, Marc Timme, and Vito Latora. Dynamically induced cascading
486 failures in power grids. *Nature communications*, pages 1–13, 2018. 8
- 487 [54] Joshua W Busby, Kyri Baker, Morgan D Bazilian, Alex Q Gilbert, Emily Grubert, Varun Rai,
488 Joshua D Rhodes, Sarang Shidore, Caitlin A Smith, and Michael E Webber. Cascading risks:
489 Understanding the 2021 winter blackout in texas. *Energy Research & Social Science*, 2021. 8
- 490 [55] Wei Yao, Lin Jiang, Jinyu Wen, QH Wu, and Shijie Cheng. Wide-area damping controller
491 of facts devices for inter-area oscillations considering communication time delays. *IEEE*
492 *Transactions on Power Systems*, 29(1):318–329, 2013. 8
- 493 [56] Joe H Chow and Kwok W Cheung. A toolbox for power system dynamics and control engineer-
494 ing education and research. *IEEE transactions on Power Systems*, 7(4):1559–1564, 1992. 8,
495 15
- 496 [57] Adam Paszke, Sam Gross, Francisco Massa, Adam Lerer, James Bradbury, Gregory Chanan,
497 Trevor Killeen, Zeming Lin, Natalia Gimelshein, Luca Antiga, et al. Pytorch: An imperative
498 style, high-performance deep learning library. *Advances in neural information processing*
499 *systems*, 32, 2019. 8
- 500 [58] Joe H Chow. *Power system coherency and model reduction*, volume 84. Springer, 2013. 9

6 Appendix

Notations. The vectors a_j, e_j respectively denote the j^{th} column of the adjacency matrix, Adj and a vector of standard basis in \mathbb{R}^m . The notation, $(a_j)_i$ denotes the i^{th} entry of the column vector a_j . I_m denote the identity matrix of size m . The Kronecker product is denoted by \otimes . The block diagonal matrix with block matrices, M_1, M_2, \dots, M_ℓ is denoted by $blkdiag(M_1, M_2, \dots, M_\ell)$.

Suppose $D = [D_1^\top \ D_2^\top \ \dots \ D_\ell^\top]^\top$ where D_1, D_2, \dots, D_ℓ are wide rectangular matrices. Then from the definition of the Frobenius norm, we have,

$$\| D \|_F^2 = \sum_{i=1}^{\ell} \| D_i \|_F^2. \quad (\text{S1})$$

If D_1 and D_2 are two matrices, then

$$\| D_1 - D_2 \|_F^2 = \| D_1 \|_F^2 + \| D_2 \|_F^2 - 2\text{trace}(D_1^\top D_2) \quad (\text{S2})$$

where $\text{trace}(D_1^\top D_2)$ denote the Frobenius inner product of the matrices D_1 and D_2 . For any matrix D , the Moore-Penrose inverse is denoted by D^\dagger .

6.1 Proof of Theorem 3

Proof. Consider the centralized learning problem described in Eq. M3 (where the notation ‘M’ indicates the equation is from the main manuscript). This problem is now rewritten with respect to each agent as follows.

$$\begin{aligned} \| Y_f - AY_p - BU \|_F^2 &= \left\| \begin{bmatrix} Y_{f,1} - A_1 Y_p - B_1 U_1 \\ Y_{f,2} - A_2 Y_p - B_2 U_2 \\ \vdots \\ Y_{f,n_a} - A_{n_a} Y_p - B_{n_a} U_{n_a} \end{bmatrix} \right\|_F^2 = \sum_{\alpha=1}^{n_a} \| Y_{f,\alpha} - A_\alpha Y_p - B_\alpha U_\alpha \|_F^2 \quad (\text{from Eq. S1}) \\ &= \sum_{\alpha=1}^{n_a} \| Y_{f,\alpha} - A_{\mathcal{N}(\alpha)} Y_{p,\mathcal{N}(\alpha)} - B_\alpha U_\alpha - A_{\overline{\mathcal{N}(\alpha)}} Y_{p,\overline{\mathcal{N}(\alpha)}} \|_F^2 \quad (\text{from Remark 2}) \\ &= \sum_{\alpha=1}^{n_a} \| Y_{f,\alpha} - A_{\mathcal{N}(\alpha)} Y_{p,\mathcal{N}(\alpha)} - B_\alpha U_\alpha \|_F^2 + \| A_{\overline{\mathcal{N}(\alpha)}} Y_{p,\overline{\mathcal{N}(\alpha)}} \|_F^2 \\ &\quad - 2 \text{trace} \left((Y_{f,\alpha} - A_{\mathcal{N}(\alpha)} Y_{p,\mathcal{N}(\alpha)} - B_\alpha U_\alpha)^\top A_{\overline{\mathcal{N}(\alpha)}} Y_{p,\overline{\mathcal{N}(\alpha)}} \right) \quad (\text{from Eq. S2}) \\ &= \sum_{\alpha=1}^{n_a} \| Y_{f,\alpha} - A_{\mathcal{N}(\alpha)} Y_{p,\mathcal{N}(\alpha)} - B_\alpha U_\alpha \|_F^2 \end{aligned}$$

where the last step follows by noticing that $A_{\overline{\mathcal{N}(\alpha)}} = 0$ since the agent α is not connected to the agents in $\overline{\mathcal{N}(\alpha)}$. In the above steps, the computation of $Y_{f,\alpha}$ and $Y_{p,\mathcal{N}(\alpha)}$ involves computing the transformation matrices $T_{f,\alpha}, R_{f,\alpha}, T_{p,\alpha}, R_{p,\alpha}$ which are computed under the knowledge of the network topology.

Finally, we obtain,

$$\begin{aligned} \min_{A,B} \| Y_f - AY_p - BU \|_F^2 &= \min_{A_{\mathcal{N}(\alpha)}, B_\alpha} \sum_{\alpha \in \{1,2,\dots,n_a\}} \| Y_{f,\alpha} - A_{\mathcal{N}(\alpha)} Y_{p,\mathcal{N}(\alpha)} - B_\alpha U_\alpha \|_F^2 \\ &= \sum_{\alpha=1}^{n_a} \min_{A_{\mathcal{N}(\alpha)}, B_\alpha} \| Y_{f,\alpha} - A_{\mathcal{N}(\alpha)} Y_{p,\mathcal{N}(\alpha)} - B_\alpha U_\alpha \|_F^2 \end{aligned}$$

For every $\alpha \in \{1, 2, \dots, n_a\}$, $A_{\mathcal{N}(\alpha)}, B_\alpha$ can now be obtained analytically as $[A_{\mathcal{N}(\alpha)} \ B_\alpha] = Y_{f,\alpha} [Y_{p,\mathcal{N}(\alpha)} \ U_\alpha]^\dagger$ and the transition mapping corresponding to the agent α is given by

$$\hat{A}_\alpha = A_{\mathcal{N}(\alpha)} R_{p,\alpha}, \quad \text{for } \alpha \in \{1, 2, \dots, n_a\}.$$

Finally the distributed Koopman is given by $A_D = [\hat{A}_1^\top \ \hat{A}_2^\top \ \dots \ \hat{A}_{n_a}^\top]^\top$, input matrix is $B_D = blkdiag(B_1, B_2, \dots, B_{n_a})$. Hence the proof. \square

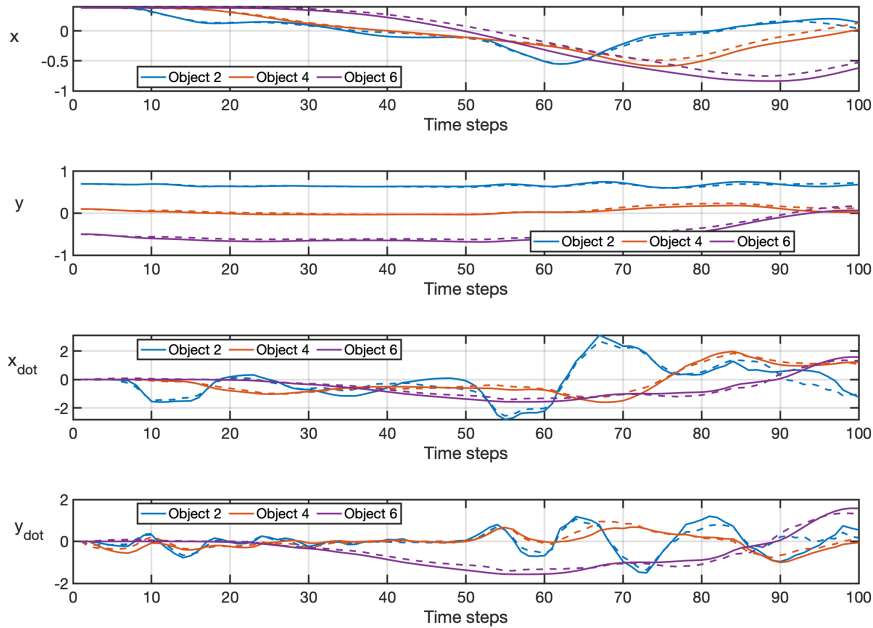


Figure 6: Rope prediction performance under random control inputs (the solid lines indicate the actual state trajectories and the dotted line shows the corresponding predictions.)

524 6.2 Proof of Corollary 4

525 *Proof.* The proof follows by noticing that in a fully connected network, for any agent α , the corre-
526 sponding non-neighbors set, $\overline{N}(\alpha)$ is empty. \square

527 6.3 More Details on the Numerical Studies

528 The network topologies of the three example systems are given in Figure 7. We follow the physics
529 simulation engine provided by [21] for generating the data for the rope example, and follow the
530 baseline node and edge attributes for the objects and connecting edges.

531 For the oscillator network, each of the individual node dynamics follows a second order differential
532 equation. The overall dynamics is represented as:

$$\begin{bmatrix} \dot{\theta} \\ \dot{\dot{\theta}} \end{bmatrix} = \begin{bmatrix} 0_{n_v} & I_{n_v} \\ -\beta M^{-1} \mathcal{L} & M^{-1} D \end{bmatrix} \begin{bmatrix} \theta \\ \dot{\theta} \end{bmatrix}, \quad (6)$$

533 where $\theta \in \mathbb{R}^{n_v}, \dot{\theta} \in \mathbb{R}^{n_v}$ are the angles and frequencies of the oscillator.
534 The diagonal matrices M and D contain inertia
535 and damping of the nodes. The coupling of the
536 nodes are captured by the Laplacian \mathcal{L} with their
537 strengths represented by β . 0_{n_v} and I_{n_v} denote
538 the zero and identity matrices of size n_v . For the
539 oscillators we have created one-hot vector for
540 node attributes. We have divided the nodes into
541 low inertia (< 3 in appropriate units), medium
542 inertia (> 3 , but < 8), and considerably high
543 inertia (> 8), thereby creating 3-dimensional
544 node attribute vectors. The edge attributes are also one-hot vectors with 6 different types. Based

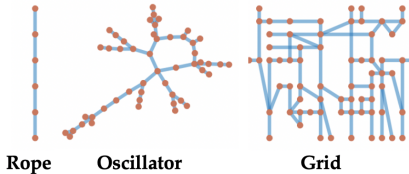


Figure 7: Network topologies

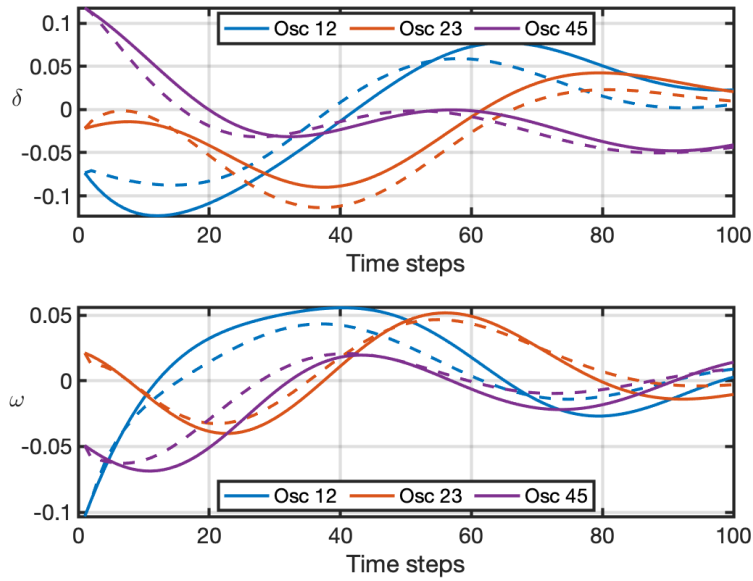


Figure 8: Oscillator prediction performance with random perturbations where the model is distributed according to the adjacency matrix of the underlying network (the solid lines indicate the actual state trajectories and the dotted line shows the corresponding predictions.)

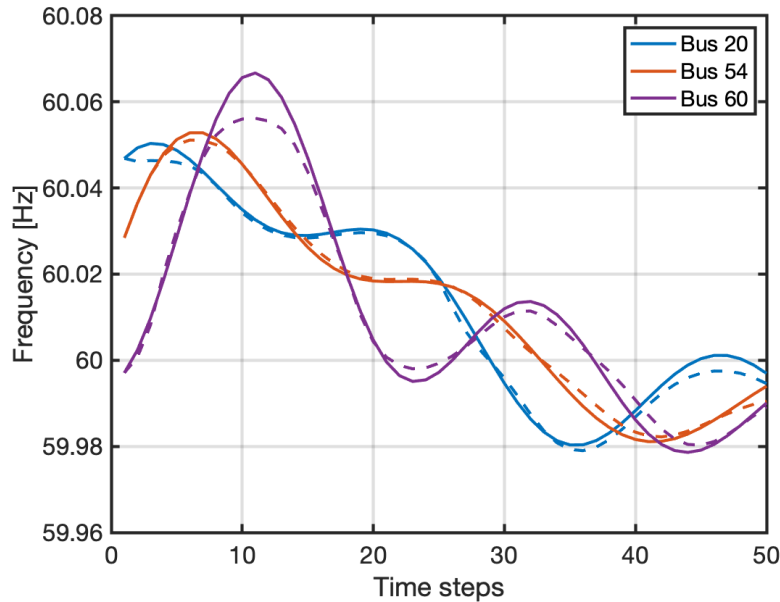


Figure 9: Powergrid prediction performance with information theoretic clustering and two-hop load perturbations (the solid lines indicate the actual state trajectories and the dotted line shows the corresponding predictions.)

545 on inertia, these types are: low-low, high-high, medium-medium, and un-directed low-medium,
546 medium-high, and low-high.

547 The IEEE benchmark 68-bus powergrid model is simulated with detailed dynamics following the
548 power system toolbox [56]. Our prediction models are learned for fast transient frequencies. The
549 node attributes are designed similarly as the oscillator studies, however, here the nodes are physical

550 powergrid buses which are classified as generator buses, load buses, and buses without any loads
551 or generators (let us call it none), thereby creating 3–dimensional one-hot vectors. The edges
552 connecting buses represent powergrid transmission lines, thereby, edge attributes are characterized as
553 generator-load, load-none, and generator-none connections, resulting in a 3–dimensional one-hot
554 vectors.

555 The network density of the systems are used to characterize the sparsity which is defined as the ratio
556 between the number of edges to the maximum number of possible edges.

557 We present few examples of the prediction performance of the DKGNN model for predicting the
558 dynamic system behaviours over time steps. Figure 6 shows the the positions and velocities of the
559 rope objects 2, 4 and 6 for the predicted performance with respect to the actual physics simulations.
560 Figure 8 shows an example of prediction performance for the network of oscillators at nodes 12, 23,
561 and 45. Prediction performance for the powergrid example is shown in Figure 9 with information-
562 theoretic clustering used for the DKGNN for buses 20, 54, and 60. These figures show satisfactory
563 performance for the distributed geometric Koopman models for all the networked dynamic system
564 examples.